This is an extended version of the paper presented in SEE7 conference, peer-reviewed again and approved by the JSEE editorial board.

Grid-Based Probabilistic Earthquake Forecast for Iran

Mohammad Talebi[1], Mehdi Zare[2*], and Anooshiravan Ansari[3]

1. Ph.D. Candidate, International Institute of Earthquake Engineering and Seismology (IIEES), Tehran, Iran
2. Professor, International Institute of Earthquake Engineering and Seismology (IIEES), Tehran, Iran, * Corresponding Author; email: mzare@iiees.ac.ir
3. Assistant Professor, International Institute of Earthquake Engineering and Seismology (IIEES), Tehran, Iran

Received: 15/08/2016
Accepted: 14/12/2016

ABSTRACT

In this paper, a model of earthquake forecast is presented to assess the long-term probabilities of future earthquakes with moderate magnitudes for a region including Iran (latitude 25-40° and longitude 44-62°). The model estimates a coupled rate of magnitude, space and time for future seismicity using a spatial-temporal Poisson process. The smoothed spatial distribution of seismicity is measured by an adaptive kernel using the locations of past $M \geq 4.5$ earthquakes listed in the ISC catalog in the period of 1980 to 2014. The retrospective area skill score test has been carried out to check the significant of the results, using a spatially uniform reference model. At 95% confidence level, the model was not rejected by the test. Moreover, the results show a meaningful correlation between anomalies of the forecasted map and the epicenters of target events occurred from 2015 to 2016. Based on the results, it is concluded that the areas characterized by high forecasted rates of seismicity could be considered as the highly hazardous ones, most likely to seismic activation in the Iranian plateau.

Keywords:
Earthquake forecast; Long-term probabilities of earthquakes; Isotropic adaptive kernel; Iran

1. Introduction

The Iranian plateau is one of the most seismically active regions in the world, and it frequently suffers catastrophic earthquakes. They cause heavy loss of human life along with lots of property damages because of the poor quality of constructions in Iran (e.g. [1-2]). One of the effective measures to reduce the hazards of earthquakes is to do risk/ hazard-analysis studies. Earthquake forecast as an important approach can be jointed in hazard and risk management for decision-making problems of emergency responses.

A number of techniques have been used for making earthquake forecasts on parts of the Iranian territory. These techniques consist of two main groups of studies, related to information from earthquake catalogs. The first group includes the studies of earthquake precursors such as seismic anomalies (e.g. [3-4]), in which the findings mostly associate with regional preparedness before the happening of main shocks. The second group is known as statistical approaches, which construct models regarding the possible occurrence of forthcoming target earthquakes (e.g. [5-6]). For instance, Radan et al [6] assessed the pattern informatics approach via retrospective tests for the identification of the anomalous areas of high earthquake risk in Iran and Italy. Maybodian et al [5] also applied the CN methodology for the study of

seismicity patterns in one of the most seismically active areas in Iran, namely the Zagros mountain belt. These studies can be categorized as alarm-based earthquake forecasts.

In the current study, the occurred earthquakes within Iran from 1980 to 2016 have been investigated in order to estimate the probabilities of future moderate magnitude events in a five-year period. This study proposes a grid-based probabilistic forecast for the study region, which do not incorporate tectonic information. This kind of earthquake forecast is also performed in some other regions, such as California (e.g. [7-8]), and assessed in the Collaboratory for the Study of Earthquake Predictability (CSEP) [9]. The findings of such kinds of efforts could be valuable to discover seismic anomalous areas of the study region. The results can present useful information to measure the seismic hazard not only in Iran, but also in other active tectonic regions

2. Data

In this study, the regional dataset of the International Seismological Centre (ISC) is applied. This catalog is available at http://www.isc.ac.uk/. The ISC catalog lists a large number of magnitude scales, which can be grouped into three main categories, namely tele-seismic, complementary magnitude, and local magnitude [5]. According to [10], here, the local and body wave magnitude of $M < 6$ as well as surface wave magnitude (M_S) of $M > 6$ are simply considered as moment magnitude.

For the current investigation, earthquakes were selected within a rectangular, latitude limits 23- 42° and longitude limits 42-64°, extended by 2° from the testing area in order to avoid the boarder effect [11]. The magnitude of completeness (*Mc*) of the dataset was checked by the maximum curvature function based on the study of Wiemer and Wyss [12]. Accordingly, the Mc is estimated as 4.5 at the 95% confidence level since 1980 (Figure 1).

Figure (2) shows temporal distributions of $M \geq 4.5$ earthquakes in this catalog.

It is seen that the curve of the cumulative number of earthquakes has an approximately constant slope since 1980. Hence, this part of the catalog, i.e. from 1980 to 2016, was chosen for using in the current study.

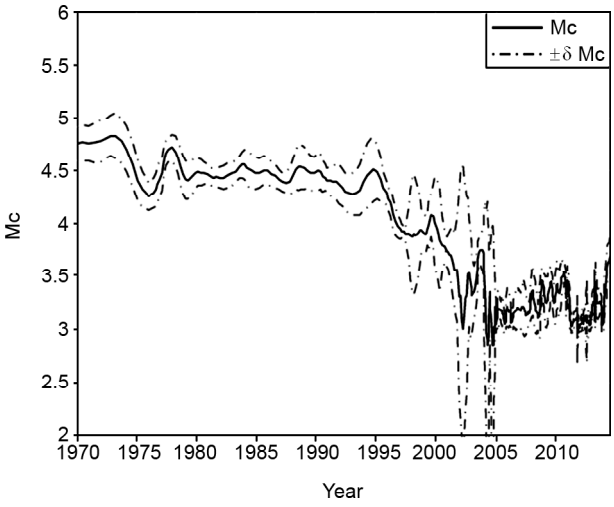

Figure 1. Magnitude completeness (Mc) of the data-set as a function of time. The Mc is estimated as 4.5 since 1980 by the maximum curvature method [12].

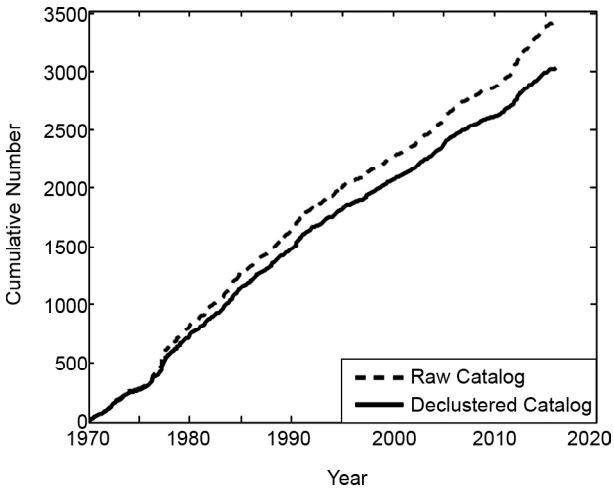

Figure 2. Temporal distribution of $M \geq 4.5$ earthquakes in the raw and declusterd catalogs. The cumulative number curve as a function of time has an approximately constant slope since 1980. The curve of the declusterd catalog has a smoother slope compared with that of the raw catalog, which illustrates that most of foreshocks and aftershocks have been removed from the catalog by the declustering procedure.

3. Declustering

In order to remove large fluctuations of seismic activity, the applied catalog was declustered by the Reasenberg's algorithm [13] as modified by Helmstetter et al [11]. The parameters of this algorithm are considered as given in [2]. The declustering procedure found ~300 earthquakes (out of ~2600 since 1980) within clusters.

Figure (1) shows temporal distribution of $M \geq$ 4.5 earthquakes in the declusterd catalog. The

cumulative number curve as a function of time for the refined catalog has a smoother slope compared with the raw catalog, which implies that the declustering procedure has removed most of the dependent events, i.e. foreshocks and aftershocks, from the catalog. The Gutenberg-Richter relation [14] for the declustered dataset was found with b-value=0.93. The tectonic earthquakes are described by the b-value in the range of 0.5 to 1.5, and the b-value is commonly around 1.0 [15]. Hence, the used dataset almost agrees with characteristic size scaling b-value.

4. Methodology

4.1. Smoothened Spatial Distribution of Seismicity

Spatial density of seismicity was estimated by smoothing the locations of $M \geq 4.5$ earthquakes. An isotropic adaptive kernel was used for smoothing past earthquake locations. As used in several studies (e.g. [11, 16]), a Gaussian type kernel was used as follows:

$$k_d(r) = C(d)\exp(-\frac{r^2}{2d^2}) \quad (1)$$

where r is epicentral distance of i-th event for each grid point, d is the adaptive scale parameter, and $C(d)$ is normalization constant set so that the integral of the kernel over an infinite area equals 1.0.

Figure (3) illustrates the use of the isotropic kernel to evaluate the smoothed rate of earthquakes. It is seen that by increasing the distance from the origin, here the point (0.5, 0.5), the smoothing function decays in space so that the contribution of an earthquake for a certain distance equals 0.0.

The bandwidth (d) of the kernel is adjusted with regard to the horizontal distance of n-th nearest neighbor of each earthquake. The number was an adaptable parameter that was evaluated by optimizing the model. The bandwidth of i-th earthquake decreased if the spatial seismic distribution was large around the location of that earthquake, so that the resolution was better where the density increased than places with low seismic density.

The density (λ) at each point was then calculated by summing the portion of all past earthquakes (N) as follows:

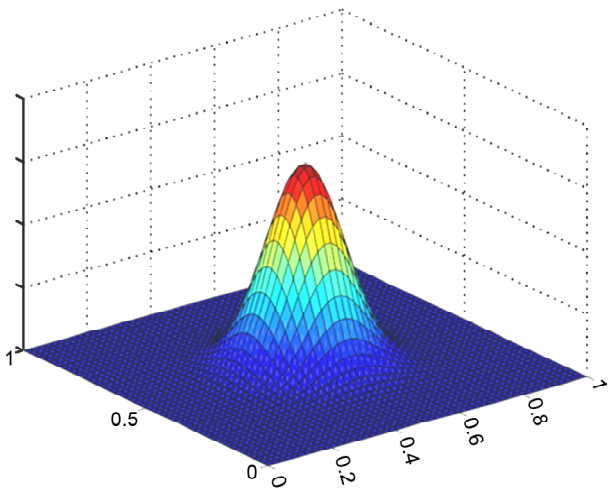

Figure 3. Schematic diagram of an isotropic Gaussian kernel. By increasing the distance from the origin, here the point (0.5, 0.5), the kernel decays in space so that the contribution of an earthquake for a certain distance equals 0.0..

$$\lambda = \sum_{i=1}^{N} K_d(r) \quad (2)$$

Finally, in order to present the number of earthquakes expected in each cell, the Eq. (2) was then integrated over each cell.

4.2. Model Optimization

The model was optimized by computing the likelihood of the model. Accordingly, a Jackknife-like procedure [7] was used in which the dataset was divided into 2 sub-catalogs. We applied the first sub-catalog, as learning catalog, to forecast the second sub-catalog, as test catalog. A large collection of catalog pairs is considered in this paper, by changing the start- and end-time and magnitude of each catalog.

In each cell (i_x, i_y), the rate λ is computed for each of the learning catalogs. Using the Eq. (3) to normalize the rates, one could estimate what part of the future earthquakes belongs to each cell:

$$\lambda^*(i_x, i_y) = \frac{\lambda(i_x, i_y) N_t}{\sum_{ix}\sum_{iy}\lambda(i_x, i_y)} \quad (3)$$

where N_t is the number of target earthquakes.

In order to assess the agreement between observed numbers of events given the expectations in each of the cells, the log-likelihoods of the models were estimated as follows [11]:

$$L = \sum_{ix} \sum_{iy} \log P[\lambda^*(i_x, i_y), n_i] \quad (4)$$

in which ni is the number of earthquakes happened in the cell (i_x, i_y).

Poisson function can be considered as the probability function (P) for the observation of n_i earthquakes in a cell with average rate λ_i^* [11]. Assuming a uniform reference model, the performance of each model is assessed by computing the probability gain per target earthquake as follows:

$$G = \exp\left(\frac{L - L_{unif}}{Nt}\right) \quad (5)$$

where L_{unif} is the log-likelihood of a spatially uniform model.

4.3. Expected Number of Earthquakes

In order to estimate the expected number of earthquakes in space-time-magnitude bins (E), the spatial density (λ) was scaled to the number of expected earthquakes over a five-year period. We have used the average number of target earthquakes over a five-year period (N_A) as the number of expected earthquakes. N_A was estimated as ~ 68 earthquakes, based on declustered catalog. Then, to estimate a magnitude-dependent rate, the scaled spatial density was multiplied by a tapered Gutenberg-Richter magnitude frequency distribution [14] as follows:

$$P(m) = 10^{-b(m-m_{\min})} \exp(10^{1.5(m_{\min}-m_c)} - 10^{-1.5(m-m_c)}) \quad (6)$$

Indeed this function, with a uniform b-value and corner magnitude mc, estimates the accumulative probability of an earthquake in each of magnitude bins. Based on [17] mc was considered to be 7.56 for Iran as an active continental region.

5. Results and Discussion

5.1. Model Parameter

The results of the model optimization are shown in Table (1), which are used to choose the model parameter k. For each model, the smoothing parameter k was varied in the range of 1 to 40 (Figure 4), and the optimal value of this parameter was selected by maximizing the likelihood of the model. A model that associates with the biggest gain has the best efficiency, and the spatially uniform model has the probability gain of 1.0. For some of

Table 1. The results of the model optimization that are used to choose the model parameters. t_f and t_l are first year and last year used to select input events, respectively; m and N are the minimum magnitude threshold and the corresponding number of events in the catalog; G is the probability gain per target earthquake over a spatially uniform model; L is the log-likelihood of the model; b_w represent the average adaptive bandwidth. The smoothing parameter k ranges between 1 and 40.

Model		Learning Catalog				Target Catalog				Result			
No	Catalog	t_f	t_l	m	N	t_f	t_l	m	N	L	G	k	b_w (km)
1	Raw	1980	1999	4.5	1289	2000	2004	5	89	-434.8	1.81	22	83
2	Raw	1980	2004	4.5	1570	2005	2009	5	72	-382.5	1.58	40	109
3	Raw	1980	2009	4.5	1802	2010	2014	5	142	-614.1	2.54	6	33
4	Raw	1980	1999	5	527	2000	2004	5	89	-436.0	1.79	23	178
5	Raw	1980	2004	5	616	2005	2009	5	72	-383.6	1.55	20	147
6	Raw	1980	2009	5	688	2010	2014	5	142	-638.7	2.13	6	58
7	Raw	1980	1999	5.5	97	2000	2004	5	89	-508.2	0.79	5	195
8	Raw	1980	2004	5.5	114	2005	2009	5	72	-407.5	1.12	3	117
9	Raw	1980	2009	5.5	126	2010	2014	5	142	-833.0	0.54	4	130
10	Declustered	1980	1999	4.5	1088	2000	2004	5	83	-402.5	2.01	40	141
11	Declustered	1980	2004	4.5	1339	2005	2009	5	63	-322.7	2.06	40	125
12	Declustered	1980	2009	4.5	1533	2010	2014	5	93	-415.2	2.78	5	34
13	Declustered	1980	1999	5	249	2000	2004	5	83	-403.4	1.99	13	198
14	Declustered	1980	2004	5	332	2005	2009	5	63	-321.5	2.10	4	72
15	Declustered	1980	2009	5	395	2010	2014	5	93	-432.7	2.30	12	141
16	Declustered	1980	1999	5.5	57	2000	2004	5	83	-503.0	0.60	7	330
17	Declustered	1980	2004	5.5	73	2005	2009	5	63	-374.6	0.90	4	190
18	Declustered	1980	2009	5.5	83	2010	2014	5	93	-556.8	0.61	6	231

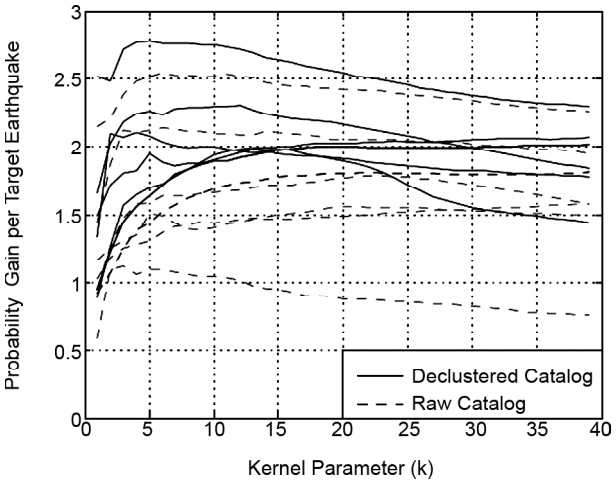

Figure 4. The selected results of the model optimization, which were used to choose the model parameter k. The optimal smoothing parameter k results in the biggest gain, and the model that associates with the biggest gain has the best efficiency. The median value of the parameter k that is used to make the final forecasts is 7.

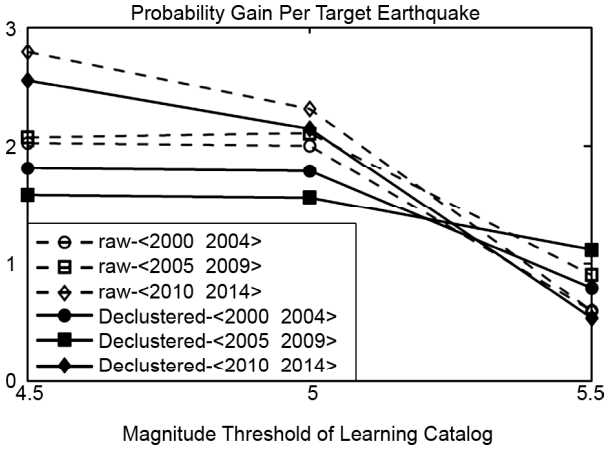

Figure 5. Model parameter choices; effects of declustering and learning magnitude threshold on the results of three different 5-year target periods (2000-2004, 2005-2009, and 2010-2014). Each curve presents the values of the probability gains obtained for the target periods.

the models, the smoothing parameter *k* reached the maximum value of 40. For those, further long-range increasing the amount of smoothing results in a uniform density [18]. Some of the models, i.e. the models 7, 9, 16, 17, and 18, provide a gain smaller than unity. All of them are related to the learning magnitude threshold of 5.5, which has small sample size less than that of target catalog. In other words, in this condition, the smoothed seismicity forecast by the Gaussian kernel does not outperform the uniform forecast.

According to Werner et al [16], the median value of the optimized parameter k (i.e. $k = 7$) has been used to make the final forecasts. Figure (5) depicts the diagrams of the probability gains per target earthquake as a function of learning magnitude threshold of the non-declustered and declustered catalogs in three different 5-year target periods (2000-2004, 2005-2009, and 2010-2014).

It is seen that there is a systematic trend for the gain versus magnitude, so that the gain decreases regularly by increasing the magnitude threshold of the learning catalogs. It means that there is a benefit on including small size events in learning catalogs. It may be due to the fact that using the largest earthquakes to train the model reduces the statistics, which can lead to ignore the location of past earthquakes with the target magnitudes. In fact, the results get very poor.

For the cases that the gain is higher than unity, it is seen that models from the declustered catalog have more gains than those made by the raw catalog. This can imply the effects of too spatial localizations of seismicity in the raw catalog on the forecast. In what follows, the declustered catalog has been used, as it has higher gains.

As mentioned previously, the average number of $M \geq 5$ events in target catalogs is ~ 68 over a five-year period. Werner et al [18] performed a similar study on two Italian catalogs. The gain values of that study fluctuate strongly as a function of input magnitude threshold in most of the target periods. In contrast to Italy with average number of ~8 events per a five-year period, the big sample size of the target earthquakes in the Iranian plateau can describe the robustness of the results of the present study.

In order to do the forecast for the predictability experiment, we decided to get advantages from as much data as possible by using all the reliable data in the dataset. Therefore, the magnitude of completeness (*Mc*) was taken as the magnitude threshold of the learning catalogs for the final forecast.

Figure (6) illustrates the forecasted seismicity rate ($M \geq 5$) map of Iran over the five-year period from 1 January 2015. By visual inspection, it seems that the forecast is consistent with most of the target events (squares whose face colors are white), which occurred in the forecast horizon until 2016.

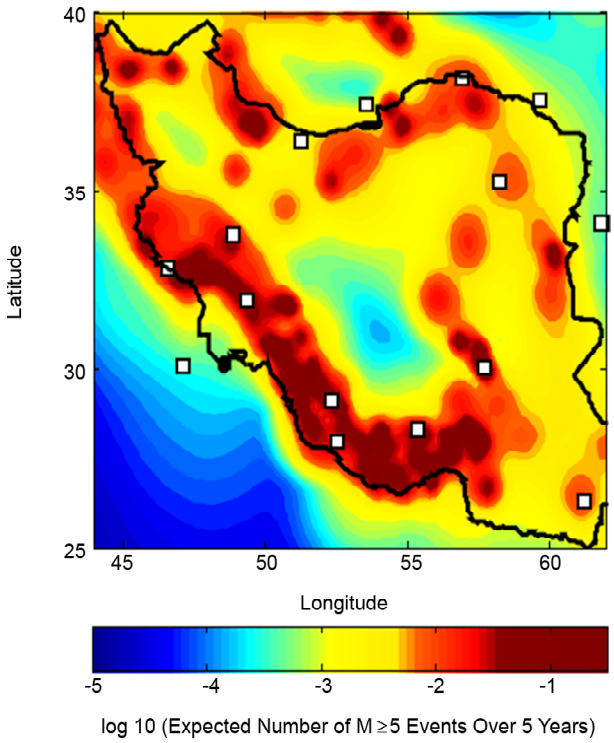

Figure 6. The base 10 logarithm of expected number of earthquakes with M ≥ 5 over the five-year period from January 1, 2015 based on smoothing the locations of earthquakes of M > 4.5 listed in the ISC catalog from 1980 to 2015. Black line shows Iran border and squares are M ≥ 5 earthquakes that occurred between January 1, 2015 and January 1, 2016.

5.2. Retrospective Tests

In order to test whether the forecast are compatible with observational data, the area skill score retrospective test was used [19, 20]. In order to do the test, the events used to estimate the spatial density were not included in the testing catalogs.

The method is basically designed for testing alarm-based earthquake forecasts and is closely related to the error diagram test [21], which is based on measuring the fraction of space volume occupied by alarm *T* against the number of target earthquakes occurred outside *T* (miss rate *v*). The water level technique [19] was also applied to change the results in a format that is suitable as the input of the area skill score test. Accordingly, by supposing a spatially uniform distribution of seismicity, a target earthquake is considered as a miss if it does not occur in an alarm cell.

The area skill score method measures the normalized space above the error diagram. The higher score of the test, the better performance of the model, so that a completely non-skilled alarm function achieves a score of 0.0, and a completely skilled one obtains a score of 1.0.

Figure (7) shows the average trajectory of the area skill scores test in three non-overlapping periods (2000-2004, 2005-2009, and 2010-2014). The shaded area displays the 95% confidence region (or α = 5% critical region), and the dashed line shows the expected values in a long run of a random guessing process. The confidence limit is estimated from the average number of target events happened in the three target periods.

It is seen that the forecasts based on the ISC catalog obtain area skill scores that are satisfactorily greater than the critical bound of area α =5% at all the points. Therefore, this test cannot reject the proposed forecasting models.

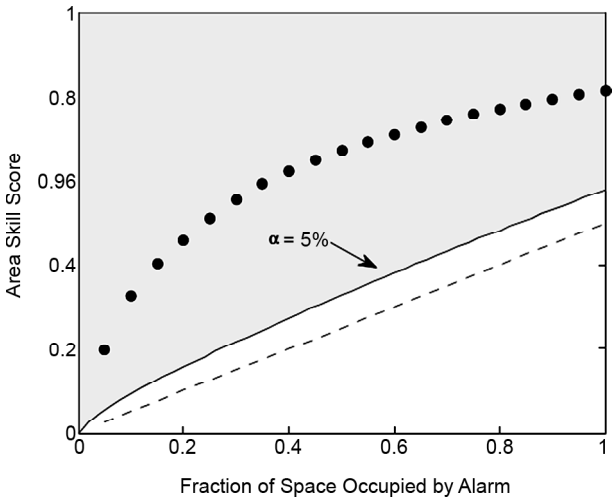

Figure 7. Average results of the retrospective area skill score test on the model in three non-overlapping periods (2000-2004, 2005-2009, and 2010-2014). The dashed lines show the long term trend of the values corresponding to random guessing. The filled area show acceptable scores at above 95% confidence (or the critical area of α = 5%).

6. Conclusion

A grid-based earthquake-forecasting model have been used to assess the probabilities of future moderate earthquakes within the Iranian territory. The model estimates a coupled rate of magnitude, space, and time for future seismicity using a spatial-temporal Poisson process. The data of ISC catalog was used in the period of 1980 to 2016. The magnitude of completeness (*Mc*) was estimated as 4.5 by the maximum curvature function. Based on optimization processes, the smallest learning

magnitude threshold of the declustered catalog was selected to make the final forecast. The area skill score retrospective test has been performed to check the consistency of the observed seismicity with the forecast. The water level method [19] has been used to adapt the format of the results with one, which is suitable for the test. Using a reference model of uniform spatial distribution, the test could not reject the forecasting model at 95% confidence level and showed that the model can serve well as a good forecast strategy.

Due to the insufficient data available, it is difficult to draw a conclusion about the possible occurrence of a big-size earthquake in the region. Moreover, a five-year forecast horizon is too short to conclude about the reliability of a large-size earthquake forecast, and a much longer time span is needed to assess the significance of related results, particularly in view of the very low forecasted rates. In other words, more than five years are necessary to check the reliability of a large-size earthquake forecast.

In total, the used model defined the most likely candidate spaces for upcoming moderate events over the five-year period from January 1, 2013. Most of these areas are found in the western and southern parts of Iran, namely Zagros zone. By passing about 2 years of forecast horizon, it is seen that there is a meaningful correlation between anomalies of the forecasted rate map of seismicity and the epicenters of target events. Based on the results and as the earthquake forecast could be an important part of hazard and risk estimations, e.g. for making decisions in risk management and emergency response, it is concluded that the anomalies of the forecasted map could be considered as highly earthquake hazardous areas that are most likely to seismic activation in the Iranian plateau.

Acknowledgment

The authors would like to thank numerous colleagues, namely, Antonella Peresan, Elham Malek Mohammadi, Ehsan Noroozinejad, and Mehdi Ahmadi Borji for sharing their points of view on the manuscript. The authors would also like to acknowledge International Institute of Earthquake Engineering and Seismology (IIEES) for its help in providing research documents and methodological aspects of the job.

References

1. Jafari, M.A. (2012) Seismicity anomalies of the 2003 Bam, Iran earthquake. *Journal of Asian Earth Sciences*, **56**, 212-217.

2. Talebi, M., Zare, M., Madahi-Zadeh, R., and Bali-Lashak, A. (2015) Spatial-temporal analysis of seismicity before the 2012 Varzeghan, Iran, Mw 6.5 earthquake. *Turkish Journal of Earth Sciences*, **24**(3).

3. Allameh-Zadeh, M., Ansari, A., Bahraminasab, A., Kaviani, K., Ardakani, A.M., Mehrnahad, H., Mehrshahi, D., Niry, M., Tabar, M., and Tabatabai, S. (2004) *Mid-Infrared Radiation as a Short-Term Earthquake Precursor*. arXiv preprint physics/0403003.

4. Mokhtari, M. (2010) Earthquake prediction activities and Damavand earthquake precursor test site in Iran. *Natural Hazards*, **52**(2), 351-368.

5. Maybodian, M., Zare, M., Hamzehloo, H., Peresan, A., Ansari, A., and Panza, G.F. (2014) Analysis of precursory seismicity patterns in Zagros (Iran) by Cn algorithm. *Turkish Journal of Earth Sciences*, **23**(1), 91-99.

6. Radan, M., Hamzehloo, H., Peresan, A., Zare, M., and Zafarani, H. (2013) Assessing performances of pattern informatics method: A retrospective analysis for Iran and Italy. *Natural Hazards*, **68**(2), 855-881.

7. Kagan, Y. and Jackson, D. (1994) Long-term probabilistic forecasting of earthquakes. *Journal of Geophysical Research*, **99**(13), 685-613, 685.

8. Kagan, Y. and Jackson, D. (2010) Short and long-term earthquake forecasts for California and Nevada. *Pure and Applied Geophysics*, **167**(6-7), 685-692.

9. Zechar, J.D., Schorlemmer, D., Liukis, M., Yu, J., Euchner, F., Maechling, P.J., and Jordan, T.H. (2010) The collaboratory for the study of earthquake predictability perspective on computational earthquake science. *Concurrency and Computation: Practice and Experience*, **22**(12), 1836-1847.

10. Zaré, M. (1999) "Contribution à l'étude des mouvements forts en Iran: du catalogue aux lois d'atténuation. Géophysique [physics.geo-ph]. Université Joseph-Fourier - Grenoble I, Français.

11. Helmstetter, A., Kagan, Y.Y., and Jackson, D.D. (2007) High-resolution time-independent grid-based forecast for $M \geq 5$ earthquakes in California. *Seismological Research Letters*, **78**(1), 78-86.

12. Wiemer, S. and Wyss, M. (2000) Minimum magnitude of completeness in earthquake catalogs: examples from Alaska, the western United States, and Japan. *Bulletin of the Seismological Society of America*, **90**(4), 859-869.

13. Reasenberg, P. (1985) Second-order moment of central California seismicity, 1969-1982. *Journal of Geophysical Research*, **90**(B7), 5479-5495.

14. Gutenberg, B. and Richter, C.F. (1944) Frequency of earthquakes in California. *Bulletin of the Seismological Society of America*, **34**(4), 185-188.

15. Mogi, K. (1967) Earthquakes and fractures. *Tectonophysics*, **5**(1), 35-55.

16. Werner, M.J., Helmstetter, A., Jackson, D.D., and Kagan, Y.Y. (2011) High-resolution long-term and short-term earthquake forecasts for California. *Bulletin of the Seismological Society of America*, **101**(4), 1630-1648.

17. Bird, P. and Kagan, Y.Y. (2004) Plate-tectonic analysis of shallow seismicity: apparent boundary width, beta, corner magnitude, coupled lithosphere thickness, and coupling in seven tectonic settings. *Bulletin of the Seismological Society of America*, **94**(6), 2380-2399.

18. Werner, M.J., Helmstetter, A., Jackson, D.D., Kagan, Y.Y., and Wiemer, S. (2010) *Adaptively Smoothed Seismicity Earthquake Forecasts for Italy*. arXiv preprint arXiv:1003.4374.

19. Zechar, J.D. and Jordan, T.H. (2008) Testing Alarm-Based Earthquake Predictions. *Geophysical Journal International*, **172**(2), 715-724.

20. Kagan, Y.Y. and Jackson, D.D. (2006) Comment on 'Testing earthquake prediction methods: "The West Pacific short-term forecast of earthquakesw with magnitude MwHRV $\geq$ 5.8"' by V.G. Kossobokov. *Tectonophysics*, **413**(1), 33-38.

21. Molchan, G.M. (1991) Structure of optimal strategies in earthquake prediction. *Tectonophysics*, **193**(4), 267-276.